ACS NANO

www.acsnano.org

ARTICLE

Optical Microscope Based Universal Parameter for Identifying Layer Number in Two-Dimensional Materials

Mainak Mondal, Ajit K. Dash, and Akshay Singh*

Cite This: *ACS Nano* 2022, 16, 14456–14462

Read Online

ACCESS | Metrics & More | Article Recommendations | Supporting Information

ABSTRACT: Optical contrast is the most common preliminary method to identify layer number of two-dimensional (2D) materials, but it is seldom used as a confirmatory technique. We explain the reason for variation of optical contrast between imaging systems, motivating system-independent measurement of optical contrast as a critical need. We describe a universal method to quantify the layer number using the RGB (red–green–blue) and RAW optical images. For RGB images, the slope of 2D flake (MoS_2, WSe_2, graphene) intensity vs substrate intensity is extracted from optical images with varying lamp power. The intensity slope identifies layer number and is system independent. For RAW images, intensity slopes and intensity ratios are completely system and intensity independent. Intensity slope (for RGB) and intensity ratio (for RAW) are thus universal parameters for identifying layer number. The RAW format is not present in all imaging systems, but it can confirm layer number using a single optical image, making it a rapid and system-independent universal method. A Fresnel-reflectance-based optical model provides an excellent match with experiments. Furthermore, we have created a MATLAB-based graphical user interface that can identify layer number rapidly. This technique is expected to accelerate the preparation of heterostructures and to fulfill a prolonged need for universal optical contrast method.

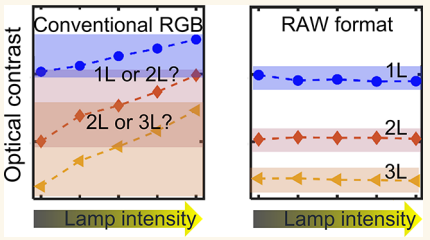

KEYWORDS: *two-dimensional materials, layer number, optical contrast, universal method, optical microscopy*

INTRODUCTION

Two-dimensional (2D) materials consist of single or few atomic layers of materials with interesting optoelectronic properties.[1,2] There is vast potential of 2D materials for sensing,[3−5] quantum computing,[6,7] and study of moiré physics.[8,9] Single or few-layer samples can be prepared through top-down (mechanical[10] and chemical exfoliation) or bottom-up (chemical vapor deposition[11]) methods. Mechanical exfoliation is the most common process for creating high-quality 2D material flakes. However, exfoliation produces randomly distributed flakes over the substrate, with varying layer number. The layer number is identified by various methods, including Raman spectroscopy, atomic force microscope (AFM), photoluminescence (PL), or optical contrast. Raman spectroscopy, AFM, or PL setups consist of sophisticated machinery and dedicated systems. The layer identification methods thus make the device preparation process slower and more costly, especially for multilayer stacked samples.[12] On the other hand, the optical contrast method only needs a simple optical microscope imaging system, making this method highly efficient and low cost.

Numerous studies discuss the identification of layer number by using optical microscope images. The changes between substrate intensity (I_{Sub}) and the 2D material flake intensity (I_F) for individual red, green, and blue channels, or the average of these channels, can identify different layered regions.[13,14] Specifically, the contrast difference ($C_D = \frac{(I_{Sub} - I_F)}{(I_{Sub} + I_F)}$ or $\frac{(I_{Sub} - I_F)}{I_{Sub}}$) measured for different channels, is used for layer identification.[15−18] C_D parameters are based on the intensity ratio (α) between I_F and I_{Sub} ($C_D = \frac{1-\alpha}{1+\alpha}$ or $1 - \alpha$), thus we only focus on α. In these studies across different laboratories and imaging systems, separate imaging conditions are maintained. As a result, optical contrast is only used for quick identification purposes instead of final confirmation.

This study aims to identify an easily accessible and universal parameter to measure layer number. We image mechanically exfoliated MoS_2 flakes (on 285 nm SiO_2/Si substrate, and also on PDMS and sapphire) using different imaging systems, in RGB and RAW formats. In the case of RGB images, we find

Received: May 17, 2022
Accepted: September 2, 2022
Published: September 8, 2022

that α can identify layer number within the same imaging system, but values of α (for a fixed layer number) vary across different imaging systems. Also, there is significant change in α for images taken with different lamp powers. We realize that the unavoidable postprocessing effects introduced during digital RGB image formation cause such variations in α. We find that I_F and I_{Sub} vary linearly (for a large intensity range) for the images taken with increasing light intensities (for both RGB and RAW formats) and that the calculated intensity slopes (μ) vary with layer number. Interestingly, the μ values for RGB format remained consistent for different imaging systems. For the RAW format, μ (as well as α) were found to be completely independent of microscope systems and the lamp power. A Fresnel-reflectance-based imaging model is used to calculate and confirm the measured α values based on RAW image formation. Hence, we suggest that intensity slope (for RGB) and intensity ratio (for RAW) can be used universally to identify layer number with high confidence. We extended the technique to graphene and WSe_2 as well with similar consistency. Finally, we have created a MATLAB-based GUI to check the slope values and confirm different layered regions quickly, allowing wide adoption of this method.

Thus, using simple optical microscopes, present in every lab doing research on 2D materials, we show on multiple 2D materials and different imaging systems that we can bypass techniques like Raman, PL, and AFM to confirm layer number. The use of RAW imaging format provides a rapid confirmatory layer identification process using a single optical image.

RESULTS AND DISCUSSION

We start with mechanically exfoliated MoS_2 on the 285 nm SiO_2/Si substrate, imaged by imaging system IS1 (see Table 1 for details on imaging systems), shown in Figure 1a. Regions with different optical contrast are expected to be regions with different layer numbers (labeled as R1, R2, and R3; substrate labeled as S). To identify the layer number, Raman spectroscopy is performed (shown in Figure 1b). The peak separation of the in-plane (E_{2g}^1) and out-of-plane (A_{1g}) vibrational mode characterizes the regions R1, R2, and R3 as monolayer (ML), bilayer (BL), and trilayer (TL), respectively.[19,20]

Table 1. Component Details for the Different Microscope Imaging Systems Used in This Study

imaging system	microscope model	light source	camera
IS1	Leica DM2500M	halogen	Leica CMOS DFC400
IS2	Olympus BX51	halogen	Olympus CCD UC30
IS3	custom built	halogen	Amscope CMOS MU1803
IS4	Olympus BX53M	white LED	Amscope CMOS MU1803

The intensity ratios (α) are calculated from the substrate (I_{Sub}) and flake intensity (I_F) for the red, green, and blue channels. Red, green and blue channel corresponds to 550−700, 450−650, and 400−550 nm, respectively (see inset of Figure 4a). The procedure of extracting these intensity values is described in Supporting Information, Section 1. For MoS_2, the calculated reflectance difference between flake and substrate regions is highest in the 550−700 nm range, corresponding to the red channel[15] (Supporting Information, Section 6). As a result, images from the red channel show the most noticeable changes in α for different layer-numbered regions. Comparison of α for different channels is shown in Figure S1. The red channel α for ML, BL, and TL MoS_2 flake (shown in Figure 1a), corresponding to images taken using four different microscope imaging systems, are plotted in Figure 1c. Change of the imaging system causes significant variations in α values, which will lead to incorrect identification of layer number. For example, α measured for ML using IS4 is the same as α measured for BL using IS2. Even for the same system, α has considerable dependence on imaging light intensity (discussed later, Figure 3b). Hence α and C_D parameters cannot be used universally to identify layer number.

Next, images of the sample are taken at different lamp powers using the imaging system IS1. I_F is found to vary linearly with I_{Sub}, with the three different layer-numbered regions having three different μ (Figure 1d). Note that these μ values are quite distinct and can differentiate between different layer-numbered regions. Next, another set of similar images is taken using IS2, IS3, and IS4. The μ values are same for ML, independent of imaging systems (Figure 1e, substrate intensity range 95−160). We also note that the intercepts are different for all the microscope systems, which results in significant α variation; see Supporting Information, Section 2, for a detailed discussion. A similar analysis is repeated for other regions, and μ values are shown in Figure 1f. For BL and TL, μ is also found to be nearly system-independent (Figure 1f). This suggests that sample−substrate intensity slopes can be used as a universal parameter to identify different layer-numbered regions accurately. Note that all the images are taken with objectives of similar numerical aperture (NA). Using objectives with different NA results in different intensity slopes (shown in Supporting Information, Section 3 and Table S1).[21−24] The mean and standard deviation of intensity slope for different flakes, across all imaging systems, are given in Supporting Information, Section 9.

To demonstrate the robustness of our technique, we have performed slope determination method on mechanically exfoliated WSe_2 and graphene flakes. The optical images of the flakes and corresponding PL[25] and Raman spectrum[26] for layer identification are given in Supporting Information, Section 4. Similar to MoS_2, WSe_2 has the highest contrast for red channel images, whereas green channel is used for graphene (Supporting Information, Section 6).[27−31] Figure 2a shows the red channel μ for ML, BL, and TL regions of WSe_2 flakes on 285 nm SiO_2/Si substrate. μ measured using different imaging systems for WSe_2 is shown in Figure 2b, which again demonstrates the nearly system-independent nature of intensity slopes. For graphene, we follow the same procedure using green channel images, and find different μ values for regions with different layer numbers (ML, BL and TL, shown in Figure 2c). The difference between intensity slopes for different layer-numbered regions in graphene is not as high as for MoS_2 and WSe_2, which is possibly related to the lower thickness of graphene layers. Figure 2d again demonstrates the nearly system-independent measurement of intensity slopes, now in the case of graphene.

Though I_F vs I_{Sub} is linear in the thus far discussed intensity range (Figure 1e) for IS3, nonlinearities are observed when measuring a larger intensity range. Total intensity range variation is plotted in Figure 3a for ML, BL, and TL regions of MoS_2 flake (same as Figure 1) for RGB. To illustrate the nonlinearity with lamp power variation, we have fitted the intensity values with a second order polynomial (solid curves

https://doi.org/10.1021/acsnano.2c04833
ACS Nano 2022, 16, 14456−14462

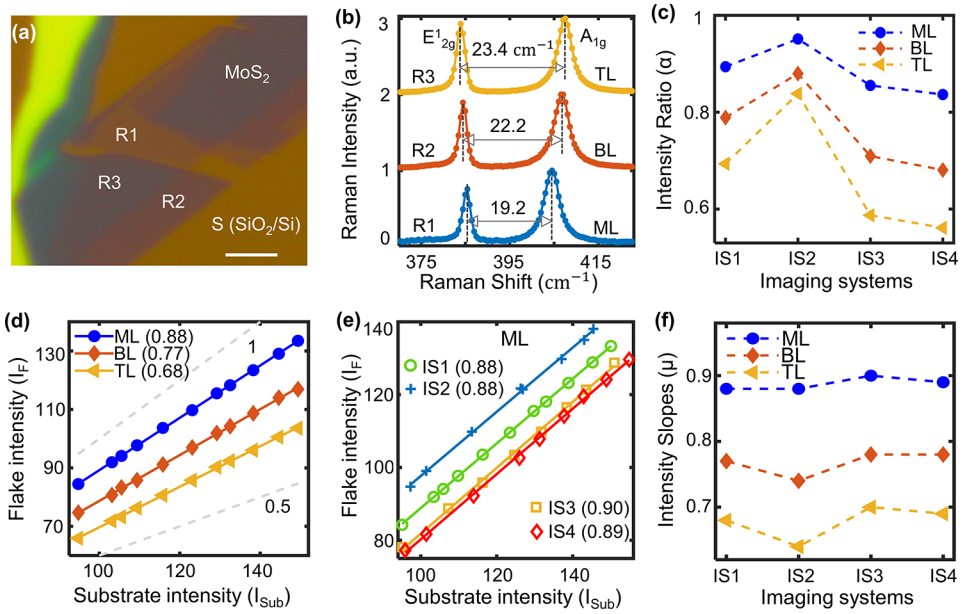

Figure 1. Intensity ratio and slope analysis for MoS_2 RGB images taken using different Imaging systems. (a) Optical image of mechanically exfoliated MoS_2 on a 285 nm SiO_2/Si substrate. Regions with different color contrasts are labeled as S (substrate), R1, R2, and R3. The scale bar is 5 μm. (b) Raman peak separation of E_{2g}^1 and A_{1g} vibrational modes for R1, R2, and R3, identifying the regions as monolayer (ML), bilayer (BL), and trilayer (TL), respectively. (c) Variation of red channel intensity ratios (α) measured using four different imaging systems (IS1, IS2, IS3, and IS4). (d) Variation of the reflected flake (ML, BL, TL) intensity (I_F) with substrate intensity (I_{Sub}) for increasing lamp light power. Intensity slopes (μ) of each line are indicated in labels. Lines of slopes 1 and 0.5 are drawn to improve visualization. (e) I_F vs I_{Sub} for ML, measured using the different imaging systems. The labels are written in the format: imaging system (slope). (f) μ for ML, BL, and TL regions measured using the different imaging systems that showed consistency across different imaging systems.

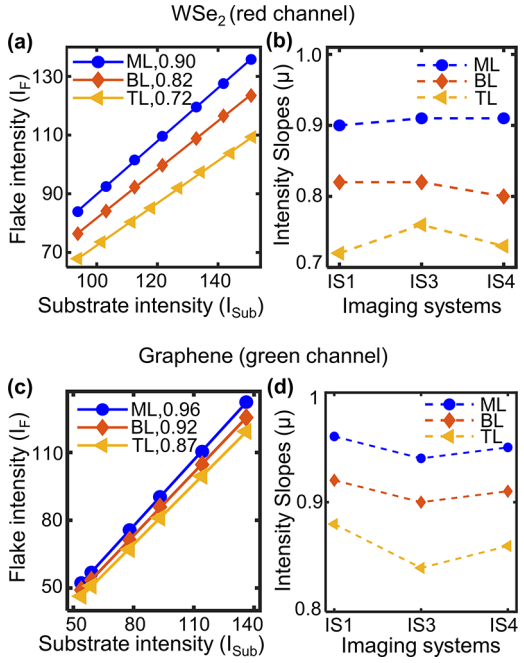

Figure 2. Intensity slope analysis for WSe_2 and graphene RGB images taken using different imaging systems. (a and c) Flake intensity variation with substrate intensity, taken in RGB format, for WSe_2 and graphene flakes, respectively. The variation is shown with linear fitting for each region. WSe_2 data uses red channel, and graphene uses green channel. (b and d) μ for red and green channels, for WSe_2 and graphene flakes, respectively, measured using different imaging systems.

in Figure 3a), $(P_1x^2 + P_2x + P_3)$. The ratio of the second and first order coefficient (P_1/P_2) represents the magnitude of nonlinearity of the intensity variations. The corresponding α is shown in Figure 3b with increasing lamp power (up to saturation of RGB pixel value, 255). These data are extracted from the images taken using IS3; similar dependence is found for IS4 (detailed comparison for all systems is given in Supporting Information, Section 2.). Both systems have the same camera and software but with different light sources (Table 1). The change in α is possibly related to the analog-to-digital conversion process of camera sensor data performed by the camera software, which includes compression, white balance, and gamma correction. This processing enables the mapping to the color and intensity range of human vision, although this conversion is nonlinear.[32,33]

To avoid these image processing-related effects, we took RAW format images, which only record the intensity data collected by camera sensors.[32,33] Intensity plots extracted from the RAW image format are shown in Figure 3c with linear best-fits. The intensity dependence is completely linear for the whole range of lamp power with nearly zero intercepts. The α values extracted from RAW images are plotted in Figure 3d, showing almost no change with increasing lamp power (data for IS4 is shown in Supporting Information, Section 5). Thus, we reason that the nonlinearity inherent to image processing and the nonzero intercept of I_F vs I_{Sub} plots (see Supporting Information, Section 2) are the causes for the significant change of α with lamp power (in case of RGB images). The intensity slope is intensity and system independent and is truly a universal parameter to characterize layer number when using the RAW format. More importantly, intensity slope and ratio are the same for RAW images, and hence α can directly be used to identify the layer number. We thus propose that RAW format images are more reliable for measuring intensity slopes than the RGB format. However, we have discussed the RGB

https://doi.org/10.1021/acsnano.2c04833
ACS Nano 2022, 16, 14456−14462

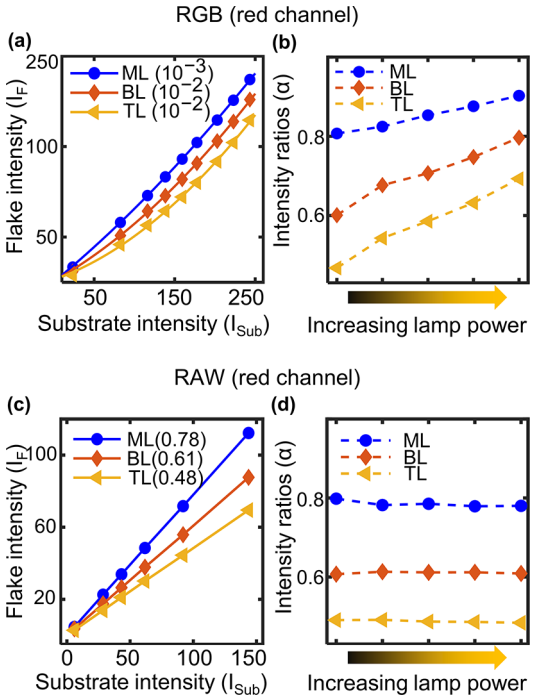

Figure 3. Intensity and slope comparison of RGB and RAW format imaging. Variation of MoS_2 flake (same as in Figure 1) intensity with substrate intensity, for red channel images, taken in RGB and RAW format, respectively. (a) Variation for RGB format shown with second order polynomial fitting ($P_1x^2 + P_2x + P_3$). P_1/P_2 values shown in the labels represent the magnitude of nonlinearity in the variation. (c) Variation for RAW format shown with linear fitting and slopes mentioned in the labels. (b and d) The α for RGB and RAW format, respectively, with increasing lamp power. All images are taken using IS3.

format due to the unavailability of RAW image capturing option in some imaging systems.

We now propose an optical model to describe the imaging system. Figure 4a is the schematic of the model, indicating the major components of a microscope imaging setup, along with sample and substrate. Reflectance of a sample region depends on the thickness of the 2D material (number of layers), the thickness of the underlying SiO_2 layer (or other substrates), and the corresponding materials' refractive indices. The Fresnel reflectance, calculated by incorporating the above parameters, is shown in Figure 4b.[34] MoS_2, SiO_2, and Si refractive indices have been reliably measured in the literature, and we directly use these values.[16,35,36] We have also calculated reflectance using the transfer matrix method and found the same results for both methods (details of the calculations can be found in Supporting Information, Section 6).[37−40] Spectrum of lamp ($L(\lambda)$) depends on the type of lamp (halogen, LED). Spectrum of halogen lamp (used in IS3) at different lamp powers is shown in Figure 4c. The reflected light spectrum ($R(\lambda) \times L(\lambda)$) results in different color for different regions. This reflected light gets detected by the camera sensor, with different sensitivities for red, green, and blue channels (sensitivity curves of a typical CMOS camera are shown in the inset of Figure 4a). Thus, the integrated output of each channel can be expressed as an intensity integral, which represents the pixel values for different channels

$$I_R = \int R(\lambda)^* L(\lambda)^* r(\lambda)^* \, d\lambda + c_r$$

$$I_G = \int R(\lambda)^* L(\lambda)^* g(\lambda)^* \, d\lambda + c_g$$

$$I_B = \int R(\lambda)^* L(\lambda)^* b(\lambda)^* \, d\lambda + c_b$$

where c is the dark count of the system.[41] Here, c is taken to be zero for RAW images (nonzero for RGB). The integrated I_R intensity values at different lamp powers are normalized with the maximum intensity value (substrate region at highest lamp power) and plotted in Figure 4d, for the different layer numbered regions. To compare the optical model with experiments, we used RAW image data (shown in Figure 3c) to avoid image-processing effects associated with RGB format.[32,33] The experimentally found intensity slopes are nearly identical with the calculated values, Figure 4e. Similar agreement of calculation and experiment is found for MoS_2 on PDMS and on sapphire substrate (shown in Supporting Information, Section 7), and also for hBN on 285 nm SiO_2/Si substrate (shown in Supporting Information, Section 10).[42−46]

To simplify the adoption of this technique for researchers, we have developed a graphical user interface (GUI) by using MATLAB (flowchart of the GUI is shown in Figure 5a), named SLOPEY. SLOPEY can be used to quickly analyze RGB (RAW) format images to check local slope (ratio) values, and to get a slope (ratio) map. For the RGB format, images at multiple lamp powers are needed as input (Figure 5b), whereas a single image is sufficient for the RAW format (Figure 5c). Next, the substrate region must be selected for both cases. From the input, SLOPEY can produce a slope map for RGB format (Figure 5d) and a ratio map for RAW format images (Figure 5e). These slope and ratio values give direct confirmation of the layer number with high confidence.

CONCLUSION

In this study, we have developed a universal parameter that can be used for determination of layer number, irrespective of the microscope system, for conventionally used RGB and RAW formats. We have found that the simplicity of conventional optical contrast methods come at the cost of reliability. Here, we discuss why the intensity ratio (and C_D) is not a reliable parameter for the RGB format, whereas it suffices for the RAW format. For RGB, the intensity slope is found to be linear for the lamp power range usually used to image a sample. For some systems, where the intensity variations are not linear throughout the intensity range (like S3 and S4), the RAW format can be an excellent solution that gives completely system and intensity-independent slope values. We also calculate slopes and ratios using a Fresnel-reflectance model and verify our measurements. We have developed a GUI, where we create a slope (or ratio) map for a specified region of interest. Through this study, we have satisfied the longstanding need for a confirmatory universal optical contrast method.

This slope method and the provided GUI do not need any special equipment, making it ready to be adopted in any lab with an optical microscope. We believe this process can be extended to any 2D materials. Database of slope and ratio values can be created for different 2D materials on different substrates. This method is expected to accelerate the identification of layer number and reduce the fabrication time of heterostructures.

https://doi.org/10.1021/acsnano.2c04833
ACS Nano 2022, 16, 14456−14462

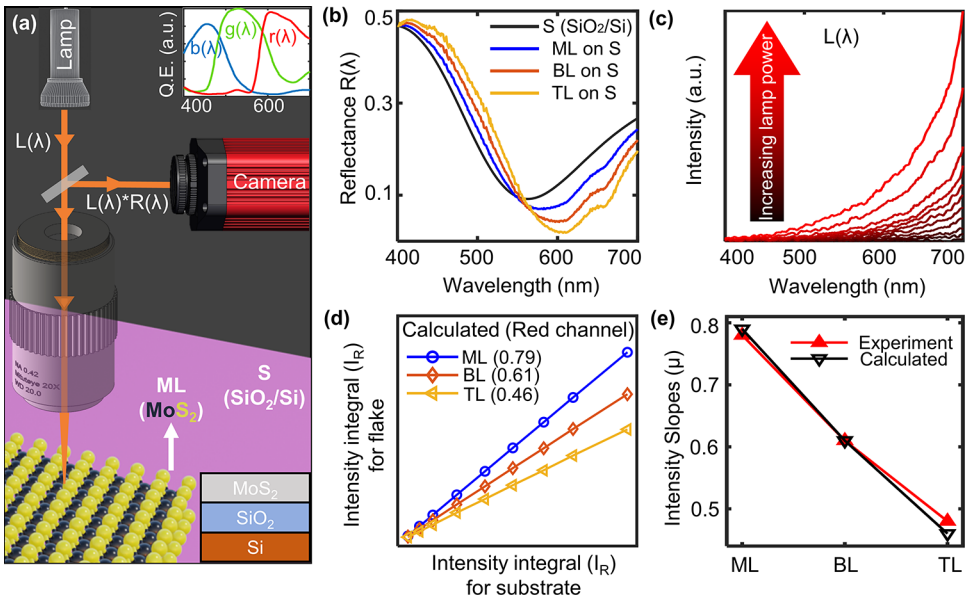

Figure 4. A Fresnel-reflectance-based optical model for calculation of the intensity slopes and comparison with experimentally measured values. (a) Schematic of optical model used for calculation of intensity slopes. The top inset shows quantum efficiency (Q.E.) curves for different channels of a typical CMOS camera sensor (shown data is for CS126CU color CMOS camera sensor). The bottom inset is structural schematic of our system. (b) Calculated reflectance of 285 nm SiO_2/Si substrate (black line), and ML, BL, and TL MoS_2 on substrate (S). (c) Halogen lamp spectrum measured by spectrometer (see methods) at different lamp powers (normalized with the highest intensity). (d) Calculated intensity integral (I_R) of reflected light for substrate, and ML, BL, and TL (on S), with increasing light intensity. Here, only red channel is shown at different lamp intensities (slopes are mentioned for each region in the legend, same as the ratio). (e) Comparison of calculated (black line) and experimentally measured (red line) μ values for RAW images.

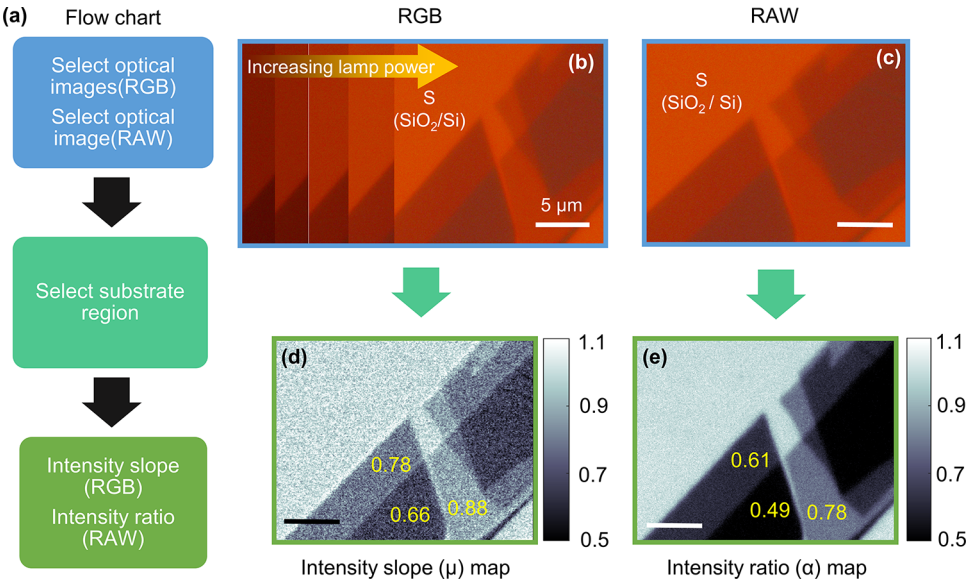

Figure 5. Graphical user interface (GUI) flowchart and examples for RGB and RAW images. (a) Flowchart of the GUI. (b and d) RGB format: Multiple images (at different lamp powers) of MoS_2 flake on SiO_2/Si substrate given as input in the GUI, output is slope (μ) map of the image. S(SiO_2/Si) is the substrate region. Slopes of different regions are mentioned in the figure. (c and e) RAW format: A single image is given as input, and output is a ratio (α) map. The ratios of different regions are mentioned on the map. Both examples are for the red channel. All the scale bars are 5 μm.

METHODS

Sample Preparation. MoS_2 and WSe_2 bulk crystals are purchased from 2D Semiconductors, and graphene is from NGS Naturgraphit GmbH. MoS_2, WSe_2 and graphene bulk crystals are exfoliated using conventional scotch tape method. We transferred graphene flakes directly to the substrate from the scotch tape. For the TMDs, we have used cell phone PET film screen protectors to transfer the flakes.

Optical Measurements. Flakes on SiO_2/Si substrate are imaged using different optical imaging systems, list is given in Table 1. The spectrum of halogen lamp at different lamp powers are taken using Kymera-328iB1 spectrometer equipped with Andor iDUS-416 CCD. All Raman and PL measurements are done using 532 nm laser in a Horiba LabRAM HR setup. The procedure to extract intensity values from the images are discussed in Supporting Information, Section 1.

https://doi.org/10.1021/acsnano.2c04833
ACS Nano 2022, 16, 14456−14462

Fresnel and Transfer Matrix Calculation. Details of the calculations can be found in Supporting Information, Section 6.

ASSOCIATED CONTENT

Supporting Information

The Supporting Information is available free of charge at https://pubs.acs.org/doi/10.1021/acsnano.2c04833.

Section 1, extraction of mean intensity values of different regions from the images; Section 2, large range intensity and ratio variation for IS1, IS2, and IS4; Section 3, variation of slope values with changing numerical aperture; Section 4, photoluminescence and Raman measurements of WSe2 and graphene; Section 5, RAW channel data for IS4 and intensity ratio comparison for different imaging systems; Section 6, Fresnel reflectance model calculations and comparison with transfer matrix formalism; Section 7, reflectance calculations and intensity ratio measurement for MoS_2 on PDMS and on sapphire substrates; Section 8, calculated intensity ratio for MoS_2 layers on SiO_2/Si substrate with varying SiO_2 thickness; Section 9, mean and standard deviation of intensity slope values across all imaging systems; and Section 10, intensity ratio for hBN on 285 nm SiO_2/Si substrate(PDF)

AUTHOR INFORMATION

Corresponding Author

Akshay Singh − *Department of Physics, Indian Institute of Science, Bengaluru 560012, India;* orcid.org/0000-0003-1059-065X; Email: aksy@iisc.ac.in

Authors

Mainak Mondal − *Department of Physics, Indian Institute of Science, Bengaluru 560012, India*

Ajit K. Dash − *Department of Physics, Indian Institute of Science, Bengaluru 560012, India*

Complete contact information is available at: https://pubs.acs.org/10.1021/acsnano.2c04833

Author Contributions

M.M. and A.S. developed the experimental and theoretical framework. M.M. performed the optical experiments and mechanical exfoliation, with assistance from A.K.D. M.M. performed the data analysis. M.M. and A.S. discussed and prepared the manuscript, with contributions from A.K.D.

Notes

The authors declare no competing financial interest.

All data are available upon reasonable request. The computer code concerning the MATLAB GUI has been uploaded at https://github.com/ousumsPhysics/SLOPEY.

The preprint version of this work is Mondal, M.; Dash, A. K.; Singh, A. Optical MicroscopeBased Universal Parameter for Identifying Layer Number in Two-DimensionalMaterials. *arXiv* 2022; doi.org/10.48550/arXiv.2204.12745 (accessed 08/30/2022).

Submissions for the ratio and slopes database can be contributed at https://forms.gle/U3SzwRttvVGT78YH6.

ACKNOWLEDGMENTS

A.S. would like to acknowledge funding from an Indian Institute of Science start-up grant. A.K.D. would like to acknowledge a Prime Minister's Research Fellowship (PMRF). The authors acknowledge Arindam Ghosh for the access of imaging system IS2. The authors also acknowledge Micro Nano Characterization Facility (MNCF), Centre for Nano Science and Engineering (CeNSE), for the use of characterization facilities.

REFERENCES

(1) Wang, G.; Chernikov, A.; Glazov, M. M.; Heinz, T. F.; Marie, X.; Amand, T.; Urbaszek, B. Colloquium: Excitons in Atomically Thin Transition Metal Dichalcogenides. *Rev. Mod. Phys.* **2018**, *90* (2), 021001.

(2) Tran, K.; Choi, J.; Singh, A. Moiré and beyond in Transition Metal Dichalcogenide Twisted Bilayers. *2D Mater.* **2021**, *8* (2), 022002.

(3) Lopez-Sanchez, O.; Lembke, D.; Kayci, M.; Radenovic, A.; Kis, A. Ultrasensitive Photodetectors Based on Monolayer MoS2. *Nat. Nanotechnol.* **2013**, *8* (7), 497−501.

(4) Yan, J.; Kim, M.-H.; Elle, J. A.; Sushkov, A. B.; Jenkins, G. S.; Milchberg, H. M.; Fuhrer, M. S.; Drew, H. D. Dual-Gated Bilayer Graphene Hot-Electron Bolometer. *Nat. Nanotechnol.* **2012**, *7* (7), 472−478.

(5) Gottscholl, A.; Diez, M.; Soltamov, V.; Kasper, C.; Krauße, D.; Sperlich, A.; Kianinia, M.; Bradac, C.; Aharonovich, I.; Dyakonov, V. Spin Defects in HBN as Promising Temperature, Pressure and Magnetic Field Quantum Sensors. *Nat. Commun.* **2021**, *12* (1), 4480.

(6) He, Y.-M.; Clark, G.; Schaibley, J. R.; He, Y.; Chen, M.-C.; Wei, Y.-J.; Ding, X.; Zhang, Q.; Yao, W.; Xu, X.; Lu, C.-Y.; Pan, J.-W. Single Quantum Emitters in Monolayer Semiconductors. *Nat. Nanotechnol.* **2015**, *10* (6), 497−502.

(7) Parto, K.; Azzam, S. I.; Banerjee, K.; Moody, G. Defect and Strain Engineering of Monolayer WSe2 Enables Site-Controlled Single-Photon Emission up to 150 K. *Nat. Commun.* **2021**, *12* (1), 3585.

(8) Regan, E. C.; Wang, D.; Jin, C.; Bakti Utama, M. I.; Gao, B.; Wei, X.; Zhao, S.; Zhao, W.; Zhang, Z.; Yumigeta, K.; Blei, M.; Carlström, J. D.; Watanabe, K.; Taniguchi, T.; Tongay, S.; Crommie, M.; Zettl, A.; Wang, F. Mott and Generalized Wigner Crystal States in WSe2/WS2Moiré Superlattices. *Nature* **2020**, *579* (7799), 359−363.

(9) Baek, H.; Brotons-Gisbert, M.; Campbell, A.; Vitale, V.; Lischner, J.; Watanabe, K.; Taniguchi, T.; Gerardot, B. D. Optical Read-out of Coulomb Staircases in a Moiré Superlattice via Trapped Interlayer Trions. *Nat. Nanotechnol.* **2021**, *16* (11), 1237−1243.

(10) Ottaviano, L.; Palleschi, S.; Perrozzi, F.; D'Olimpio, G.; Priante, F.; Donarelli, M.; Benassi, P.; Nardone, M.; Gonchigsuren, M.; Gombosuren, M.; Lucia, A.; Moccia, G.; Cacioppo, O. A. Mechanical Exfoliation and Layer Number Identification of MoS 2 Revisited. *2D Mater.* **2017**, *4* (4), 045013.

(11) Huang, J.-K.; Pu, J.; Hsu, C.-L.; Chiu, M.-H.; Juang, Z.-Y.; Chang, Y.-H.; Chang, W.-H.; Iwasa, Y.; Takenobu, T.; Li, L.-J. Large-Area Synthesis of Highly Crystalline WSe2Monolayers and Device Applications. *ACS Nano* **2014**, *8* (1), 923−930.

(12) Bing, D.; Wang, Y.; Bai, J.; Du, R.; Wu, G.; Liu, L. Optical Contrast for Identifying the Thickness of Two-Dimensional Materials. *Opt. Commun.* **2018**, *406*, 128−138.

(13) Li, H.; Wu, J.; Huang, X.; Lu, G.; Yang, J.; Lu, X.; Xiong, Q.; Zhang, H. Rapid and Reliable Thickness Identification of Two-Dimensional Nanosheets Using Optical Microscopy. *ACS Nano* **2013**, *7* (11), 10344−10353.

(14) Li, H.; Lu, G.; Yin, Z.; He, Q.; Li, H.; Zhang, Q.; Zhang, H. Optical Identification of Single- and Few-Layer MoS2 Sheets. *Small* **2012**, *8* (5), 682−686.

(15) Li, Y.; Kong, Y.; Peng, J.; Yu, C.; Li, Z.; Li, P.; Liu, Y.; Gao, C.-F.; Wu, R. Rapid Identification of Two-Dimensional Materials via Machine Learning Assisted Optic Microscopy. *Journal of Materiomics* **2019**, *5* (3), 413−421.

(16) Zhang, H.; Ma, Y.; Wan, Y.; Rong, X.; Xie, Z.; Wang, W.; Dai, L. Measuring the Refractive Index of Highly Crystalline Monolayer MoS 2 with High Confidence. *Sci. Rep* **2015**, *5* (1), 8440.

(17) Li, Y.; Dong, N.; Zhang, S.; Wang, K.; Zhang, L.; Wang, J. Optical Identification of Layered MoS2via the Characteristic Matrix Method. *Nanoscale* **2016**, *8* (2), 1210−1215.
(18) Late, D. J.; Liu, B.; Matte, H. S. S. R.; Rao, C. N. R.; Dravid, V. P. Rapid Characterization of Ultrathin Layers of Chalcogenides on SiO2/Si Substrates. *Adv. Funct. Mater.* **2012**, *22* (9), 1894−1905.
(19) Lee, C.; Yan, H.; Brus, L. E.; Heinz, T. F.; Hone, J.; Ryu, S. Anomalous Lattice Vibrations of Single- and Few-Layer MoS2. *ACS Nano* **2010**, *4* (5), 2695−2700.
(20) Li, H.; Zhang, Q.; Yap, C. C. R.; Tay, B. K.; Edwin, T. H. T.; Olivier, A.; Baillargeat, D. From Bulk to Monolayer MoS2: Evolution of Raman Scattering. *Adv. Funct. Mater.* **2012**, *22* (7), 1385−1390.
(21) Saigal, N.; Mukherjee, A.; Sugunakar, V.; Ghosh, S. Angle of Incidence Averaging in Reflectance Measurements with Optical Microscopes for Studying Layered Two-Dimensional Materials. *Rev. Sci. Instrum.* **2014**, *85* (7), 073105.
(22) Gao, L.; Ren, W.; Li, F.; Cheng, H.-M. Total Color Difference for Rapid and Accurate Identification of Graphene. *ACS Nano* **2008**, *2* (8), 1625−1633.
(23) Menon, T. S.; Mishra, S.; Antony, V. C.; Dixit, K.; Kakkar, S.; Ahmed, T.; Islam, S.; Jayaraman, A.; Hsieh, K.; Karnatak, P.; Ghosh, A. Optimising Graphene Visibility in van Der Waals Heterostructures. *Nanotechnology* **2019**, *30* (39), 395704.
(24) Hutzler, A.; Fritsch, B.; Matthus, C. D.; Jank, M. P. M.; Rommel, M. Highly Accurate Determination of Heterogeneously Stacked Van-Der-Waals Materials by Optical Microspectroscopy. *Sci. Rep* **2020**, *10* (1), 13676.
(25) Li, Y.; Li, X.; Yu, T.; Yang, G.; Chen, H.; Zhang, C.; Feng, Q.; Ma, J.; Liu, W.; Xu, H.; Liu, Y.; Liu, X. Accurate Identification of Layer Number for Few-Layer WS2 and WSe2 via Spectroscopic Study. *Nanotechnology* **2018**, *29* (12), 124001.
(26) Graf, D.; Molitor, F.; Ensslin, K.; Stampfer, C.; Jungen, A.; Hierold, C.; Wirtz, L. Spatially Resolved Raman Spectroscopy of Single- and Few-Layer Graphene. *Nano Lett.* **2007**, *7* (2), 238−242.
(27) Wang, Y. Y.; Gao, R. X.; Ni, Z. H.; He, H.; Guo, S. P.; Yang, H. P.; Cong, C. X.; Yu, T. Thickness Identification of Two-Dimensional Materials by Optical Imaging. *Nanotechnology* **2012**, *23* (49), 495713.
(28) Jung, G.-H.; Yoo, S.; Park, Q.-H. Measuring the Optical Permittivity of Two-Dimensional Materials without a Priori Knowledge of Electronic Transitions. *Nanophotonics* **2018**, *8* (2), 263−270.
(29) Weber, J. W.; Calado, V. E.; van de Sanden, M. C. M. Optical Constants of Graphene Measured by Spectroscopic Ellipsometry. *Appl. Phys. Lett.* **2010**, *97* (9), 091904.
(30) Fang, H.; Chuang, S.; Chang, T. C.; Takei, K.; Takahashi, T.; Javey, A. High-Performance Single Layered WSe2 p-FETs with Chemically Doped Contacts. *Nano Lett.* **2012**, *12* (7), 3788−3792.
(31) Ni, Z. H.; Wang, H. M.; Kasim, J.; Fan, H. M.; Yu, T.; Wu, Y. H.; Feng, Y. P.; Shen, Z. X. Graphene Thickness Determination Using Reflection and Contrast Spectroscopy. *Nano Lett.* **2007**, *7* (9), 2758−2763.
(32) Schewe, J. *The Digital Negative: Raw Image Processing in Lightroom, Camera Raw, and Photoshop*, Second ed.; Peachpit Press: San Francisco, CA, 2016; pp 27−28.
(33) Andrews, P.; Butler, Y.; Butler, Y. J.; Farace, J. *Raw Workflow from Capture to Archives: A Complete Digital Photographer's Guide to Raw Imaging*, First ed.; Focal: Oxford. U.K., 2006; pp 3−10.
(34) Blake, P.; Hill, E. W.; Castro Neto, A. H.; Novoselov, K. S.; Jiang, D.; Yang, R.; Booth, T. J.; Geim, A. K. Making Graphene Visible. *Appl. Phys. Lett.* **2007**, *91* (6), 063124.
(35) Aspnes, D. E.; Studna, A. A. Dielectric Functions and Optical Parameters of Si, Ge, GaP, GaAs, GaSb, InP, InAs, and InSb from 1.5 to 6.0 EV. *Phys. Rev. B* **1983**, *27* (2), 985−1009.
(36) Gao, L.; Lemarchand, F.; Lequime, M. Exploitation of Multiple Incidences Spectrometric Measurements for Thin Film Reverse Engineering. *Opt. Express, OE* **2012**, *20* (14), 15734−15751.
(37) Troparevsky, M. C.; Sabau, A. S.; Lupini, A. R.; Zhang, Z. Transfer-Matrix Formalism for the Calculation of Optical Response in Multilayer Systems: From Coherent to Incoherent Interference. *Opt. Express, OE* **2010**, *18* (24), 24715−24721.
(38) Anantharaman, S. B.; Stevens, C. E.; Lynch, J.; Song, B.; Hou, J.; Zhang, H.; Jo, K.; Kumar, P.; Blancon, J.-C.; Mohite, A. D.; Hendrickson, J. R.; Jariwala, D. Self-Hybridized Polaritonic Emission from Layered Perovskites. *Nano Lett.* **2021**, *21* (14), 6245−6252.
(39) Wong, J.; Jariwala, D.; Tagliabue, G.; Tat, K.; Davoyan, A. R.; Sherrott, M. C.; Atwater, H. A. High Photovoltaic Quantum Efficiency in Ultrathin van Der Waals Heterostructures. *ACS Nano* **2017**, *11* (7), 7230−7240.
(40) Peumans, P.; Yakimov, A.; Forrest, S. R. Small Molecular Weight Organic Thin-Film Photodetectors and Solar Cells. *J. Appl. Phys.* **2003**, *93* (7), 3693−3723.
(41) Jessen, B. S.; Whelan, P. R.; Mackenzie, D. M. A.; Luo, B.; Thomsen, J. D.; Gammelgaard, L.; Booth, T. J.; Bøggild, P. Quantitative Optical Mapping of Two-Dimensional Materials. *Sci. Rep* **2018**, *8* (1), 6381.
(42) Zhang, X.; Qiu, J.; Li, X.; Zhao, J.; Liu, L. Complex Refractive Indices Measurements of Polymers in Visible and Near-Infrared Bands. *Appl. Opt., AO* **2020**, *59* (8), 2337−2344.
(43) Malitson, I. H. Refraction and Dispersion of Synthetic Sapphire. *J. Opt. Soc. Am., JOSA* **1962**, *52* (12), 1377−1379.
(44) Rah, Y.; Jin, Y.; Kim, S.; Yu, K. Optical Analysis of the Refractive Index and Birefringence of Hexagonal Boron Nitride from the Visible to Near-Infrared. *Opt. Lett., OL* **2019**, *44* (15), 3797−3800.
(45) Golla, D.; Chattrakun, K.; Watanabe, K.; Taniguchi, T.; LeRoy, B. J.; Sandhu, A. Optical Thickness Determination of Hexagonal Boron Nitride Flakes. *Appl. Phys. Lett.* **2013**, *102* (16), 161906.
(46) Kumar, P.; Lynch, J.; Song, B.; Ling, H.; Barrera, F.; Kisslinger, K.; Zhang, H.; Anantharaman, S. B.; Digani, J.; Zhu, H.; Choudhury, T. H.; McAleese, C.; Wang, X.; Conran, B. R.; Whear, O.; Motala, M. J.; Snure, M.; Muratore, C.; Redwing, J. M.; Glavin, N. R.; Stach, E. A.; Davoyan, A. R.; Jariwala, D. Light-Matter Coupling in Large-Area van Der Waals Superlattices. *Nat. Nanotechnol.* **2022**, *17* (2), 182−189.

https://doi.org/10.1021/acsnano.2c04833
ACS Nano 2022, 16, 14456−14462